JRC Scientific and Technical Reports

Landsat 7 Enhanced Thematic Mapper JRC-FAPAR Algorithm Theoretical Basis Document

Nadine Gobron and Malcolm Taberner

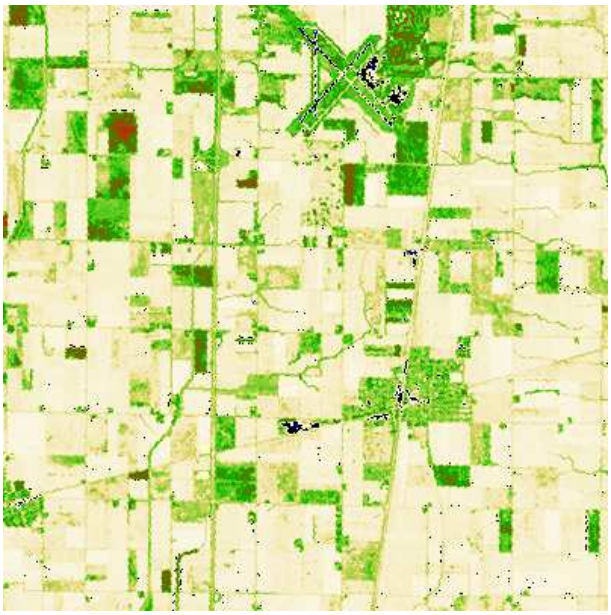

EUR No. 23554 EN -2008

The mission of the Institute for Environment and Sustainability is to provide scientific-technical support to the European Union's Policies for the protection and sustainable development of the European and global environment.

European Commission
Joint Research Centre
Institute for Environment and Sustainability

Contact information
Address: EC-JRC, TP 270, via E. Fermi, 2749
21027 Ispra (VA) Italy
E-mail: nadine.gobron@jrc.it
Tel.: +39 0332 786338
Fax: +39 0332 789073

`http://ies.jrc.ec.europa.eu`
`http://www.jrc.ec.europa.eu`

JRC 48063
EUR 23554 EN
ISSN 1018-5593
Luxembourg: Office for Official Publications of the European Communities

Printed in Italy

Contents

List of Figures

List of Tables

1. Introduction

1.1. **Purpose.** This Algorithm Theoretical Basis document (ATBd) describes the Joint Research Center (JRC)- procedure used to retrieve information of absorbed photosynthetical radiation by the vegetated terrestrial surfaces from an analysis of the Top Of Atmosphere (TOA) data acquired by the Landsat 7 Enhanced Thematic Mapper (ETM+) instrument. The corresponding data consist of eight spectral bands, with a spatial resolution of 30 meters for bands 1 to 5 and band 7 whereas the resolution for band 6 (thermal infrared) is 60 meters and resolution for band 8 (panchromatic) is 15 meters. Approximate scene size is 170 km north-south by 183 km east-west.

The code of the proposed algorithm takes the form of a set of several formulae which transform calibrated spectral directional reflectances into a single numerical value. These formulae are designed to extract the Fraction of Absorbed Photosynthetically Active Radiation (FAPAR) in the plant canopy from the measurements. The methodology described in this document has been optimized to assess the presence on the ground of healthy live green vegetation. The optimization procedure has been constrained to provide an estimate of FAPAR in the plant canopy, although the outputs are expected to be used in a wide range of applications. This algorithm delivers, in addition to the FAPAR product, the so-called rectified reflectance values in the red and near-infrared spectral bands (Landsat 7 ETM+ Band 3 and Band 4). These are virtual reflectances largely decontaminated from atmospheric and angular effects. It also provides a categorization of pixel types thanks to a pre-processing identification based on multi-spectral properties.

This document identifies the sources of input data, outlines the physical principles and mathematical background justifying this approach, describes the proposed algorithm, and lists the assumptions and limitations of this technique. Finally, one application using one image is presented for illustrating the use of this algorithm.

1.2. **Algorithm identification.** The algorithm described below is called the JRC-Landsat 7 Optimized FAPAR (JRC-L7OF). It is suitable for any surface applications requiring the monitoring of the state of the land surface.

1.3. **Scope.** This document outlines the algorithm which is recommended to generate FAPAR product and associated rectified red and near-infrared reflectance values.

1.4. **Revision history.** This document presents the first release of the JRC-Landsat 7 Optimized FAPAR algorithm (*i.e.* version 1.0).

1.5. **Other relevant documents.** Other references to technical reports, ATBds and additional information about Landsat can be found at the following internet address:
`http://landsat.gsfc.nasa.gov/`
`http://landsathandbook.gsfc.nasa.gov/`
`http://www.landsat.org/`
`http://eros.usgs.gov/products/satellite/landsat7.html`.

A series of relevant reports and articles are included in the bibliography list and the associated IDL routines implementing this algorithm are available at
`http://fapar.jrc.ec.europe.eu/`.

2. Algorithm overview

2.1. **Objectives of surface retrievals.** The bulk of the solar radiation available to the Earth system is absorbed at or near the oceanic and continental surface. This energy is ultimately released to the atmosphere through the fluxes of infrared radiation, as well as sensible and latent heat. The phytosphere, which itself accounts for most of the biomass, affects these exchanges through a surface of contact (leaves) with the atmosphere estimated to be larger than the surface of the entire planet.

The state and evolution of terrestrial vegetation is characterized by a large number of physical, biochemical and physiological variables. Few of these are directly observable from space, but they jointly determine the Fraction of Absorbed Photosynthetically Active Radiation (FAPAR) which acts as an integrated indicator of the status and health of the plant canopy, and can reasonably be retrieved by remote sensing techniques. FAPAR plays also a critical role in the biosphere path of the global carbon cycle and in the determination of the primary productivity of the phytosphere.

The properties of terrestrial surfaces thus concern a large number of users through such applications as agriculture, forestry, environmental monitoring, etc. Since plant canopies significantly affect the spectral and directional reflectance of solar radiation, it is expected that the analysis of repeated observations of these reflectances may lead to a better understanding of the fundamental processes controlling the biosphere, which, in turn, will support the definition of sustainable policies of environmental exploitation, and the control of the effectiveness of any adopted rules and regulations.

The FAPAR has been also recognized as one of the fundamental Essential Climate Variable (ECV) by Global Terrestrial Observing System (GTOS) and Global Climate Observing System (GCOS). A series of FAPAR algorithm has been optimized for various optical instrument such as SeaWiFS (Gobron et al. 2002), VEGETATION (Gobron et al. 2002b), GLobal Imager (GLI) (Gobron et al. 2002a), MERIS (Gobron et al. 2004) and MODIS (Gobron et al. 2006a) and (Gobron et al. 2006b). Validation exercises at medium resolution scale have been already performed for both SeaWiFS (Gobron et al. 2006) and MERIS (Gobron et al. 2008). Developing such a FAPAR algorithm for LANDSAT also helps for the validation against ground-based measurements which are done at few meters.

The overall scientific objective of the JRC-FAPAR algorithm is to exploit the spectral reflectance measurements acquired by solar instruments to provide users with reliable qualitative and quantitative information on the state of the plant cover over terrestrial areas. Specifically, the output value is meant to be easily interpreted in terms of FAPAR values.

The design of the JRC-FAPAR requires, in a first step, the estimate of the so-called rectified reflectances at the red and near-infrared wavelengths in order to minimize atmospheric and angular perturbations. These intermediary land surface products should

prove useful for documenting the state of the land surfaces and also assessing the spatio-temporal variations in land cover type. Specifically, these rectified reflectances correspond to the amplitude parameter of the BRF entering the Rahman, Pinty, Verstraete (RPV) parametric model (Rahman et al. 1993). These are virtual, *i.e.*, not directly measurable in the field, spectral reflectances which are, at best, decontaminated from atmospheric and angular effects.

2.2. **Instrument characteristics.** The Landsat 7 ETM+ sensor characteristics and the data are described in
`http://landsathandbook.gsfc.nasa.gov/handbook/handbook_toc.html`.

For the purpose of this document, it is sufficient to recall that Landsat-7 system is designed to collect 7 bands or channels of reflected energy and one channel of emitted energy. The three bands used in our algorithm correspond to the Band 1, 3 and 4 in the blue, red and near-infrared domain, respectively.

TABLE 1. Landsat 7 ETM+ Spectral Bandwidths

Band	Bandwidth (μ)
1	**0.45-0.52**
2	0.53-0.61
3	**0.63-0.69**
4	**0.78-0.90**
5	1.55-1.75
6	10.4-12.5
7	2.09-2.35
8	.52 - .90

Each band spectral response is illustrated in Figure 1 (the spectral responses of these bands are published at `http://landsathandbook.gsfc.nasa.gov/`). One can notice that, comparing to the latest optical sensors such as MODIS, MERIS and SeaWiFS, the bandwidth are relatively larger. The blue band encompasses the green domain and the near-infrared band contains typical gaseous transmission wavelengths and its width is double compared to the the medium resolution sensors.

The proposed algorithm will thus focus on the exploitation of the spectral variability of the data, keeping in mind the possible perturbing effects that may result from variations in geometry within and between successive images, mainly due to the sun zenith angle since the observation geometry is closed to the nadir view (less than 2° at the edge of the image).

The spatial resolution of these three Landsat 7 ETM+ bands correspond to approximately 30 meters with an overpass of 16 days.

2.3. **Retrieval approach.** The specific objective of this document is to describe the algorithm suitable to estimate FAPAR optimized for the LANDSAT 7 ETM+ instrument.

The strategy follows the ones already used for a series of optical instrument such as SeaWiFS (Gobron et al. 2002), VEGETATION (Gobron et al. 2002b), GLobal Imager (GLI) (Gobron et al. 2002a), MERIS (Gobron et al. 2004) and MODIS (Gobron et al. 2006a; Gobron et al. 2006b).

The design criteria are:

(1) to provide a high sensitivity to the Fraction of Absorbed Photosynthetically Active Radiation (FAPAR) when a vegetated area is detected,

(2) to maintain a low sensitivity to soil and atmospheric conditions whenever vegetation is detected,

(3) to exploit the multi-band specificity of the sensor,

(4) to be independent of the geometry of illumination and observation, and

(5) to offer excellent discrimination capabilities, *i.e.*, the opportunity to distinguish various target types.

(6) to be independent of the spatial resolution.

3. Algorithm description

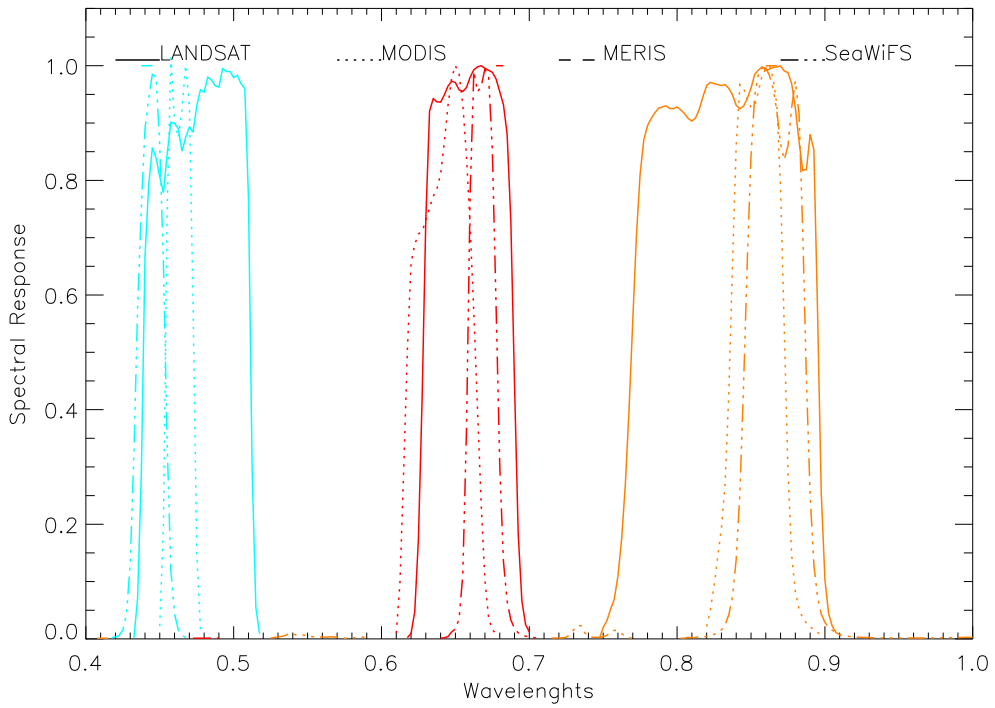

Figure 1. Spectral response of LANDSAT 7 ETM+ (full line), MODIS (dotted line), MERIS (dashed line) and SeaWiFS for their blue, red and near-infrared bands as function of the wavelengths

3.1. **Physics of the problem.** The general theory behind the design of optimal spectral indices has been described in Verstraete and Pinty (1996), and its specific application to medium resolution instruments has been addressed in Govaerts et al. (1999), Gobron et al. (1999) and Gobron et al. (2000).

The most recent implementation of the algorithm assumes that, 1) the FAPAR can be used to quantify the presence of vegetation and, 2) radiation transfer model simulations can be used to define appropriate scenarios over different representative land surfaces.

The bulk of the information on the presence of vegetation is contained *a priori* in the red and the near-infrared spectral bands, typically at wavelengths such as Band 3 and Band 4 of Landsat 7 ETM+.

Addressing the atmospheric problem consists in converting Top Of Atmosphere (TOA) Bidirectional Reflectance Factors (BRFs) into Top Of Canopy (TOC) BRFs. Two classes of atmospheric radiative processes affect the measurements made by space-borne satellites: absorption and scattering. Absorption of radiation by specific gases can be largely avoided by carefully choosing the spectral location of narrow bands. This latter condition was however difficult to achieved with high spatial resolution sensor comparing to the medium space sensors. New generation of high spatial sensors, such as Sentinel-2, should be designed to better compromise the spectral and spatial resolutions. Further corrections can be at least implemented by estimating the amount of these gases from specific spectral bands. The effect of scattering cannot be avoided, and both molecular and aerosol scattering are strongly dependent on the wavelength of radiation. Hence, measurements in the blue region of the solar spectrum will provide values much more sensitive to atmospheric scattering than at longer wavelengths. In this approach, the characterization of plant canopies over fully or partially vegetated pixels currently relies on the analysis of data in 3 Landsat 7 spectral bands, namely Band 1 at 0.45-0.52 μm, Band 3 at 0.63-0.69 μm, and Band 4 at 0.78-0.90 μm.

A Look Up Table (LUT) of bidirectional reflectance factors representing the Landsat 7 ETM+ like data has been created using the physically-based semi-discrete model of Gobron et al. (1997) to represent the spectral and directional reflectance of horizontally homogeneous plant canopies, as well as to compute the values of FAPAR in each of them. The soil data required to specify the lower boundary condition in this model were taken from Price (1995). Figure 2 illustrates various spectra soil from 'dark' to 'bright' used in the simulations.

The spectral values for the leaf reflectance and transmittance were simulated using the leaf spectral model from Jacquemoud and Baret (1990) using standard leaf properties which correspond to the following biochemical values:

- Leaf internal structure parameter = 1.75,
- Leaf chlorophyll a+b content = 48.6 $\mu g cm^{-2}$,
- Leaf equivalent water thickness = 0.0115 cm,
- Leaf protein content = 0.00096 gcm^{-2} and
- Leaf cellulose+lignin content = 0.00168 gcm^{-2}.

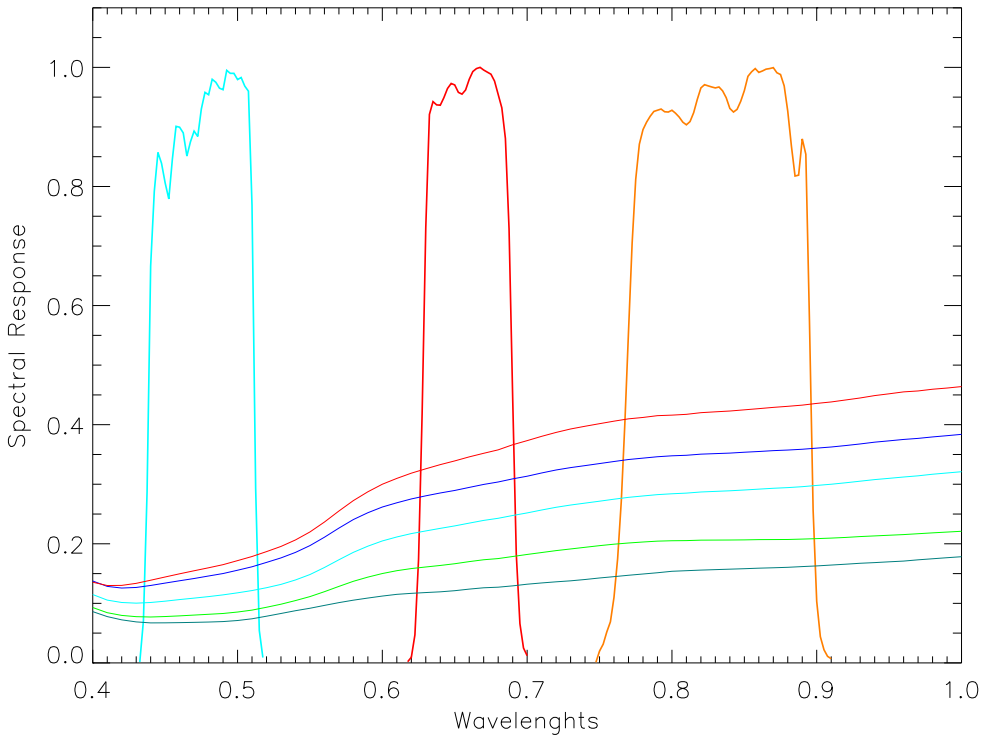

FIGURE 2. Spectral albedo of five soil (Price, 1995) used for the simulations of the training data sets.

Figure 3 shows the profile of both reflectance and transmittance of the leaf as well as reported the corresponding values in the 3 Landsat 7 ETM+ bands and in the 'visible' domain (*i.e.* domain in which FAPAR values are simulated). These values are computed by taken into account the spectral response of each band, $S_n(\lambda_i)$, as well as the solar radiation, $E_0(\lambda_i)$, using the following equation:

$$R_l(T_l) = \int_{\lambda_1}^{\lambda_2} \frac{r_l(\lambda_i) E_0(\lambda_i) S_n(\lambda_i) \delta\lambda_i}{E_0(\lambda_i) S_n(\lambda_i) \delta\lambda_i} \quad (1)$$

The Second Simulation of the Satellite Signal in the Solar Spectrum (6S) atmospheric model of Vermote et al. (1997) has been used to represent the atmospheric absorption and scattering effects on the measured reflectances. The FAPAR values are computed using the closure of the energy balance inside the plant canopy in the spectral range 400 to 700 nm. The various geophysical scenarios performed to simulate the radiance fields are summarized in Table 2 and the geometrical conditions of illumination and observation are given in Table 3. The sampling of the vegetation parameters and angular values were chosen to cover a wide range of environmental conditions. These simulations constitute the basic information used to optimize the formulae. The sampling selected to generate the LUT has been chosen so as to generate a robust global FAPAR algorithm.

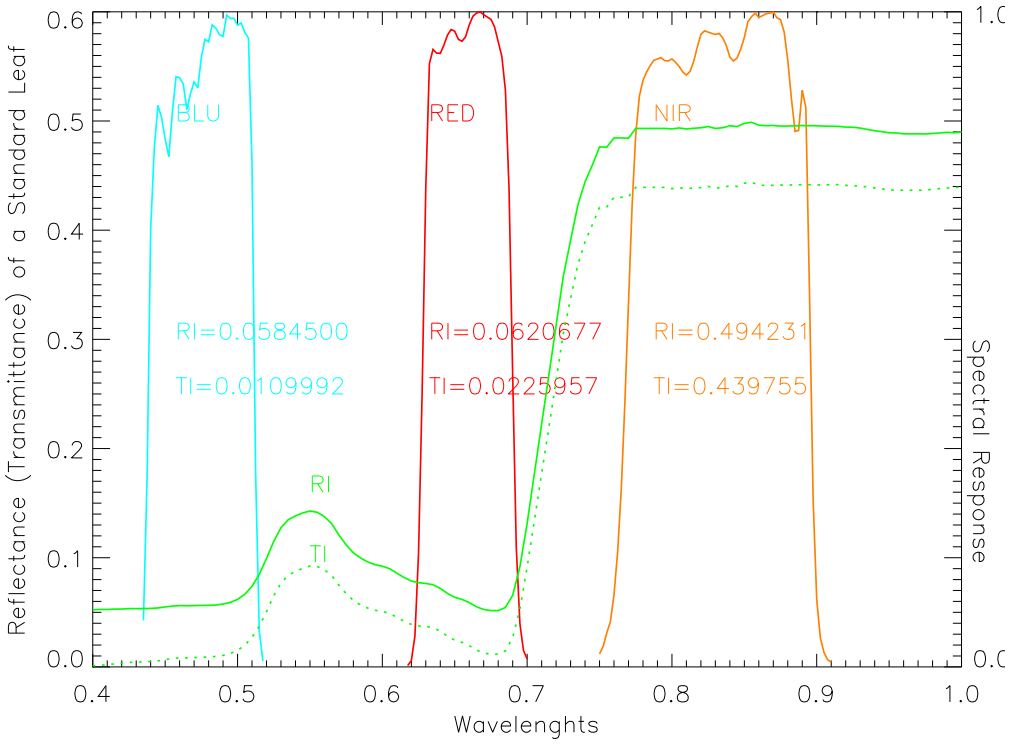

FIGURE 3. Spectral reflectance (R_l) and transmittance (T_l) of a standard leaf. The numbers indicate the convoluted values of each Landsat band used in the simulations.

TABLE 2. Geophysical scenarios used to simulate the radiance fields.

Medium	**Variable**	**Meaning**	**Range of values**
Atmosphere model (Vermote *et al.*, 1997)	τ_s	Aerosol opt. thickness	0.05, 0.3 and 0.8
Vegetation model (Gobron *et al.*, 1997)	LAI	Leaf Area Index	0, 0.5, 1, 2, 3, 4, and 5
	H_c	Height of Canopy	0.5 m and 2 m
	d_ℓ	Equivalent diameter of single leaf	0.01 m and 0.05 m
	LAD	Leaf Angle Distribution	Erectophile, Planophile
Soil data base (Price, 1995)	r_s	Soil reflectance	5 soil spectra, from dark to bright

TABLE 3. Illumination and observation geometries used to simulate the radiance fields.

Variable	**Angle**	**Values**
θ_0	Solar zenith angle	20° and 50°
θ_v	Sensor zenith angle	0°, 2°and 4°
ϕ	Sun-Sensor relative azimuth	0°, 90° and 180°

Once this LUT has been created, the design of the algorithm consists in defining the mathematical combination of spectral bands which will best account for the variations of the variable of interest (here, FAPAR) on the basis of (simulated) measurements, while minimizing the effect of perturbing factors such as atmospheric or angular effects. This process is described in the next section.

3.2. **Mathematical description of the algorithm.** The proposed algorithm to compute the FAPAR value, is organized around three main consecutive steps.

(1) As mentioned previously, because of the actual sampling strategy implemented by the Landsat 7 ETM+ instrument in the angular domain, it is not possible to retrieve the anisotropy of the radiance field. A parametric anisotropic function is implemented to account for variations in the signal due to changes in the geometrical conditions. The bidirectional reflectance model of Rahman et al. (1993) (RPV) is assumed to be appropriate for this task:

$$\rho_i(\theta_0, \theta_v, \phi) = \rho_{i0}\, F(\theta_0, \theta_v, \phi; k_i, \Theta_i^{hg}, \rho_{ic}) \tag{2}$$

where F characterizes the anisotropy of the medium in terms of three unknown parameters, namely k_i, Θ_i^{hg} and ρ_{ic} which depend exclusively on the intrinsic properties of the type of geophysical system for a given spectral band i. The function $F(\Omega; k_i, \Theta_i^{hg}, \rho_{ic})$ with $\Omega = (\theta_0, \theta_v, \phi)$ is given by:

$$F(\Omega; k_i, \Theta_i^{hg}, \rho_{ic}) = f_1(\theta_0, \theta_v, k_i)\, f_2(\Omega, \Theta_i^{hg})\, f_3(\Omega, \rho_{ic}) \tag{3}$$

where

$$f_1(\theta_0, \theta_v, k_i) = \frac{(\cos\theta_0\ \cos\theta_v)^{k_i - 1}}{(\cos\theta_0 + \cos\theta_v)^{1-k_i}} \tag{4}$$

$$f_2(\Omega, \Theta_i^{hg}) = \frac{1 - \Theta_i^{hg\,2}}{\left(1 + 2\,\Theta_i^{hg}\ \cos g + \Theta_i^{hg\,2}\right)^{3/2}} \tag{5}$$

$$f_3(\Omega, \rho_{ic}) = 1 + \frac{1 - \rho_{ic}}{1 + G} \tag{6}$$

with

$$G = \left(\tan^2\theta_0 + \tan^2\theta_v - 2\ \tan\theta_0\ \tan\theta_v\ \cos\phi\right)^{1/2} \tag{7}$$

$$\cos g = \cos\theta_0\ \cos\theta_v + \sin\theta_0\ \sin\theta_v \cos\phi \tag{8}$$

The characterization of a geophysical system with the RPV model thus requires the estimation of four parameter values, namely ρ_{i0}, k_i, Θ_i^{hg} and, ρ_{ic} which are independent of the geometry of illumination and observation Ω.

The parameters intervening in function F are optimized separately in the three bands using the simulated BRFs emerging at the top of atmosphere.

(2) The information contained in the band 1 (blue) is combined with that in the bands 3 and 4 (red and near-infrared) traditionally used to monitor vegetation, in order to generate "rectified bands" at these latter two wavelengths. The "rectification" is done in such a way as to minimize the difference between those rectified bands and

the spectral reflectances that would have been measured at the top of the canopy under identical geometrical conditions but in the absence of the atmosphere.

(3) The FAPAR value is then generated on the basis of these "rectified bands".

The proposed algorithm assumes that ratios of polynomials are appropriate to generate both the "rectified bands" with the following generic formula:

$$g_n(x,y) = \frac{l_{n,1}(x+l_{n,2})^2 + l_{n,3}(y+l_{n,4})^2 + l_{n,5}xy}{l_{n,6}(x+l_{n,7})^2 + l_{n,8}(y+l_{n,9})^2 + l_{n,10}xy + l_{n,11}} \tag{9}$$

where x and y are the spectral bands at the appropriate step. The L7OF formula itself is given by the following formulae:

$$g_0(x,y) = \frac{l_{0,1}\,y - l_{0,2}\,x - l_{0,3}}{(l_{0,4}-x)^2 + (l_{0,5}-y)^2 + l_{0,6}} \tag{10}$$

$$\text{L7OF} = g_0(\rho_{RRed}, \rho_{RNIR}) \tag{11}$$

where ρ_{RRed} and ρ_{RNIR} are the rectified reflectance values in the red and near-infrared bands described above. These, in turn, are estimated with

$$\rho_{RRed} = g_1(\tilde{\rho}_{Band1}, \tilde{\rho}_{Band3}) \tag{12}$$

$$\rho_{RNIR} = g_2(\tilde{\rho}_{Band1}, \tilde{\rho}_{Band4}) \tag{13}$$

where

$$\tilde{\rho}_i = \frac{\rho_i^*(\theta_0, \theta_v, \phi)}{F(\theta_0, \theta_v, \phi; k_i, \Theta_i^{hg}, \rho_{ic})} \tag{14}$$

and where ρ_i^* denotes the (simulated) top of atmosphere bidirectional reflectance factor in band i, while $\tilde{\rho}_i$ is the bidirectional reflectance factor normalized by the anisotropic function F. An optimization procedure is applied to retrieve successively the optimal values of the coefficients intervening in the three steps mentioned above, namely k_i, Θ_i^{hg} and ρ_{ic}, and $l_{n,j}$ for the polynomials g_n, both for the rectified bands and for the final index itself.

(1) In the first step, it is assumed that the anisotropic shapes of the BRFs simulated at the top of the atmosphere may change with the spectral wavelength of interest, but do not depend on the geophysical systems specified to generate the BRFs. Accordingly, for a given spectral band, the three parameters of the anisotropic function F are forced to be constant over the entire set of geophysical scenarios considered. In practice, this condition is achieved by minimizing the following cost functions:

$$\delta_i^2 = \sum_{\zeta,\Omega} \left[\left(\frac{\rho_i^*(\Omega)}{F(\Omega; k_i, \Theta_i^{hg}, \rho_{ic})} \right) - \tilde{\rho}_i \right]^2 \to 0 \tag{15}$$

where ζ represents the geophysical domain and Ω the angular domain over which the optimization is sought.

Since $\tilde{\rho}_i$ is assumed to be constant in the RPV model for each individual geophysical system taken separately, we can estimate the mean value of the BRFs over the Ω space for every geophysical system:

$$\frac{1}{N_{obs}} \sum_{\Omega} \rho_i^*(\Omega_j) = \frac{1}{N_{obs}} \sum_{\Omega} \tilde{\rho}_i \times F(\Omega_j; k_i, \Theta_i^{hg}, \rho_{ic}) \tag{16}$$

$$= \tilde{\rho}_i \frac{1}{N_{obs}} \sum_{\Omega} F(\Omega_j; k_i, \Theta_i^{hg}, \rho_{ic}) \tag{17}$$

where N_{obs} is the total number of angular situations. The model coefficient $\tilde{\rho}_i$ is thus approximated for each geophysical system as

$$\tilde{\rho}_i = \frac{1}{N_{obs}} \sum_{\Omega} \rho_i^*(\Omega_j) \Big/ \frac{1}{N_{obs}} \sum_{\Omega} F(\Omega_j; k_i, \Theta_i^{hg}, \rho_{ic}) \tag{18}$$

The cost function is rewritten as follows:

$$\delta_i^2 = \sum_{\zeta} \left[\frac{\rho_i^*(\Omega)}{F(\Omega; k_i, \Theta_i^{hg}, \rho_{ic})} \frac{1}{N_{obs}} \sum_{\Omega} F(\Omega_j; k_i, \Theta_i^{hg}, \rho_{ic}) - \frac{1}{N_{obs}} \sum_{\Omega} \rho_i^*(\Omega_j) \right]^2 \to 0 \tag{19}$$

(2) To satisfy the various requirements described above, the optimization procedure is applied in the Band 3 and 4 separately, to derive the coefficients of g_1 and g_2. This is achieved by minimizing the following cost functions:

$$\delta_{g_i}^2 = \sum_{\zeta} \left[g_i(\tilde{\rho}_{Blue}, \tilde{\rho}_i) - \tilde{\rho}_i^{TOC} \right]^2 \to 0. \tag{20}$$

where

$$\tilde{\rho}_i^{TOC} = \frac{\rho_i^{TOC}(\Omega)}{F(\Omega, k_i^{TOC}, \Theta_i^{hg,TOC}, \rho_{ic}^{TOC})} \tag{21}$$

for which the anisotropic parameters, namely $k_i^{TOC}, \Theta_i^{hg,TOC}, \rho_{ic}^{TOC}$, were previously optimized at the top of canopy level.

(3) Following the rectification of the BRFs in the previous step, the coefficients of g_0 are evaluated by minimizing the following cost function:

$$\delta_{g_0}^2 = \sum_{\zeta} \left[g_0(\rho_{RRed}, \rho_{RNir}) - \mathrm{FAPAR}(\mu_0) \right]^2 \to 0. \tag{22}$$

In other words, L7OF output is forced to take on values as close as possible to the $FAPAR(\mu_0)$ associated with the specified plant canopy scenarios. The simulated top-of-atmosphere spectral and directional reflectances generated by the coupled model have been exploited with an extended version of the FACOSI tool (Govaerts et al. 1999) to adjust the formulae on the basis of the given set of equations. The numerical results are summarized in Tables 4 to 7.

Figures (4) and (5) illustrate the impact of the "rectification" procedure, which combines TOA reflectances in the Band 1 with TOA reflectances in the Bands 3 and 4, respectively. The left panels on these figures show the relationships between the spectral BRFs TOC normalized by the anisotropic function F, and BRFs TOA for all geophysical and angular

TABLE 4. Values of the parameters for the anisotropic function F.

band	**Parameter values**		
	ρ_{ic}	k_i	Θ_i^{hg}
Blue (Band 3)$^{(a)}$	0.643	0.76611	−0.10055
Red (Band 1)$^{(b)}$	0.80760	0.63931	−0.06156
NIR (Band 2)$^{(a)}$	0.89472	0.81037	−0.03924

$^{(a)}$ Optimization using TOA & TOC vegetated and bare soil BRFs simulations.
$^{(b)}$ Optimization using TOA & TOC vegetated BRFs simulations.

TABLE 5. Coefficients for the polynomial g_1.

$l_{1,1}$	$l_{1,2}$	$l_{1,3}$	$l_{1,4}$	$l_{1,5}$	
−10.036	−0.019804	0.55438	0.14108	12.494	
$l_{1,6}$	$l_{1,7}$	$l_{1,8}$	$l_{1,9}$	$l_{1,10}$	$l_{1,11}$
0	0	0	0	0	1.0

$^{(a)}$ Optimization using TOA & TOC vegetated and bare soil BRFs simulations.

TABLE 6. Coefficients for the polynomial g_2.

$l_{2,1}$	$l_{2,2}$	$l_{2,3}$	$l_{2,4}$	$l_{2,5}$	
0.42720	0.069884	−0.33771	0.24690	−1.0821	
$l_{2,6}$	$l_{2,7}$	$l_{2,8}$	$l_{2,9}$	$l_{2,10}$	$l_{2,11}$
−0.30401	−1.1024	−1.2596	−0.31949	−1.4864	

$^{(a)}$ Optimization using TOA & TOC vegetated and bare soil BRFs simulations.

TABLE 7. Coefficients for the polynomial g_0.

$l_{0,1}$	$l_{0,2}$	$l_{0,3}$	$l_{0,4}$	$l_{0,5}$	$l_{0,6}$
0.27505	0.35511	−0.004	−0.322	0.299	−0.0131

$^{(a)}$ Optimization using TOA & TOC vegetated and bare soil BRFs simulations.

scenarios described in Table 2. The scattering of the points is caused by changes in the atmospheric conditions and by the relative geometry of illumination and observation. The right panels show the effect of the "rectification" process, which reduces this dispersion. A perfect "rectification" would collapse all points on the 1:1 line for each of the surface types considered. It can be seen that this process is particularly efficient over dense vegetation, and that it reduces the systematic bias due to atmospheric effects on BRFs in both bands.

Figure (6) provides information on the performance of the algorithm in term of providing FAPAR values from the BRF TOA values. The right panel shows the isolines of the JRC-L7OF values in the spectral space of the rectified bands in the red (x-axis) and near-infrared (y-axis). It can be seen that the values varies between 0 and 1 over partially and

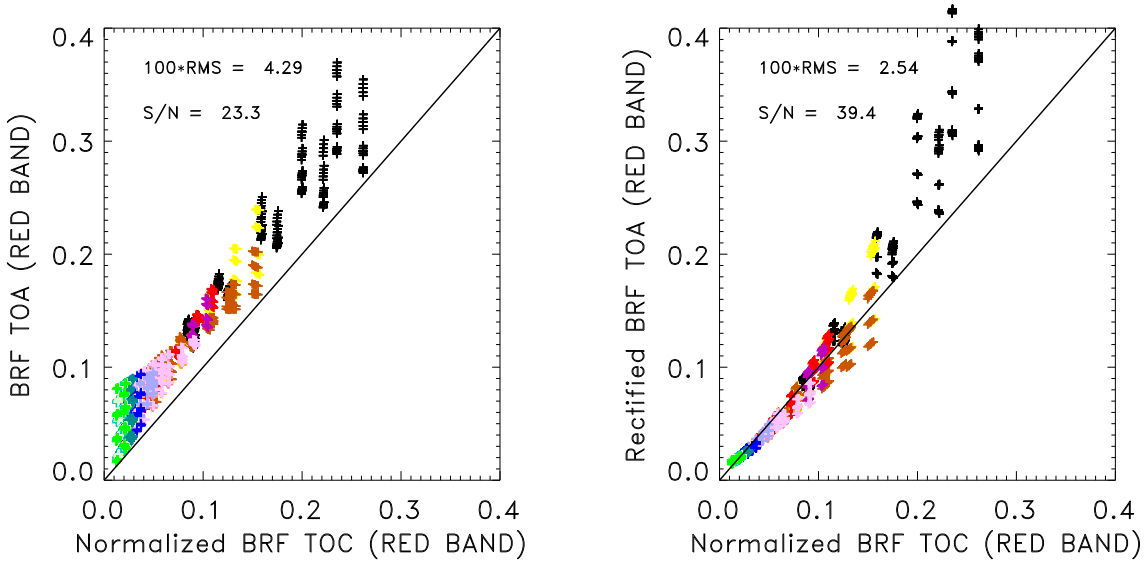

FIGURE 4. Left panel: relationship between the BRFs TOC normalized by the anisotropic function F, and BRFs TOA, for all conditions given in Table 2, in the red band. Right panel: relationship between the "rectified" reflectances and the corresponding BRFs TOC normalized by the anisotropic function F. The various colours represent different values of FAPAR for the plant canopies described in Table 2.

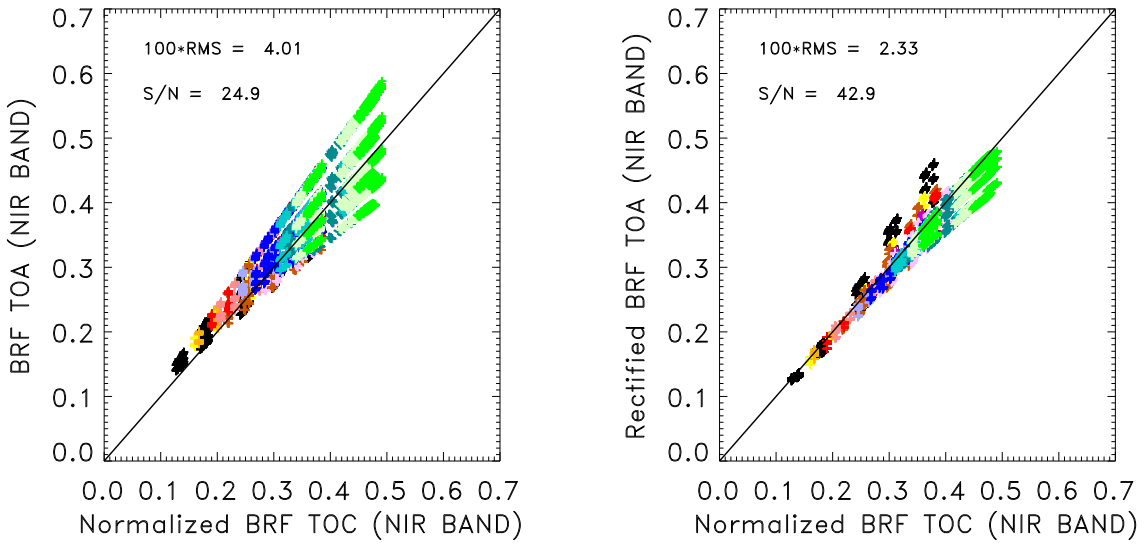

FIGURE 5. Same as Figure (4) except for the Band 2.

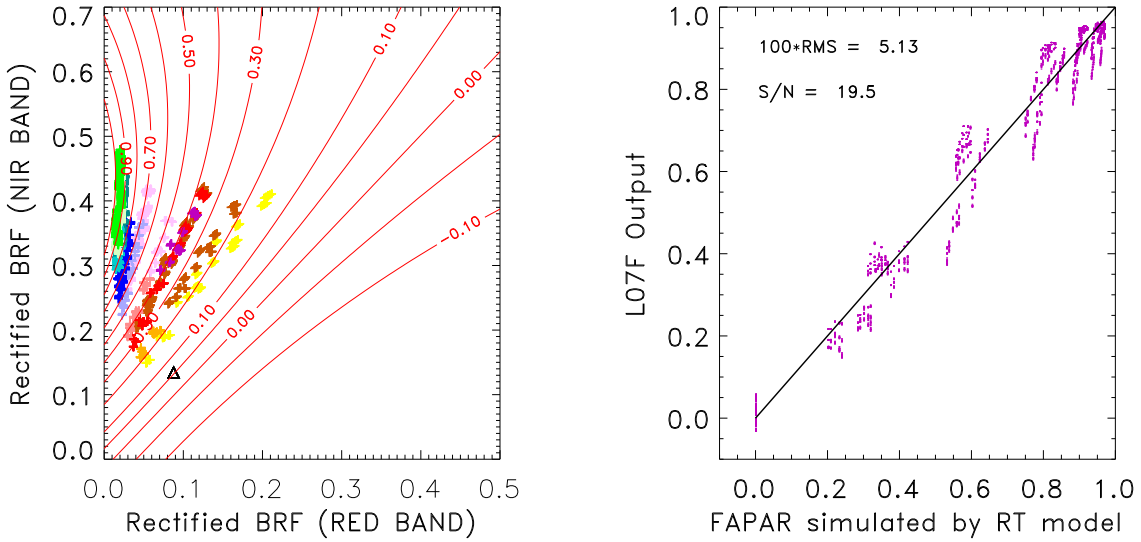

FIGURE 6. The right panel shows the isolines of JRC-L7OF in the "rectified" spectral space together with the simulated radiances at the top of the atmosphere (see Table 2).The left panel shows the relationship between the index and the FAPAR values.

fully vegetated surfaces and takes negative values out of the spectral domain of interest. The left panel of the same figure shows that JRC-L7OF output is close to the FAPAR with a root mean square deviation closed to 0.05. Most of the remaining variability is probably caused by the various conditions that were considered in the geophysical scenarios (see Table 2). In fact, this variability results from conflicting requirements on the insensitivity of the algorithm to soil, atmospheric and geometrical effects in the Landsat 7 spectral bands.

4. Error budget estimates

Since the algorithm has been optimized to provide a high sensitivity to FAPAR, a measurable biophysical variable, its capacity to detect the presence of green vegetation can be objectively assessed. For the particular geophysical scenarios in Table 2 and angular sampling given in Table 3, the root mean square deviation value of the fit between these two quantities is at about 0.05. Following the method proposed by Leprieur et al. (1994), the performance can be evaluated with the help of a signal to noise ratio. In the present case, it was found that the signal to noise ratio of the algorithm is equal to **19.5**.

4.1. **Practical considerations.**

4.1.1. *Quality control and diagnostics.* A simple approach is proposed to associate a label to each pixel of the Landsat 7 ETM + data in order to optimize the various steps of the processing to be achieved over water bodies and land surfaces.

Table 8 indicates the tests applied and the associated categories for discriminating the major geophysical systems (also identified with an identification number), namely clouds,

bright surfaces, vegetated surfaces and water bodies. In the data product, the various identification numbers correspond to a set of flag values.

As can be seen from Table 8, the pixel labeling is performed on the basis of an ensemble of thresholds using only the values in the spectral bands used in the algorithm. For each geophysical category, the ensemble of tests has been established on the basis of knowledge of the multi-spectral signatures of the geophysical systems. The proposed approach classifies the vast majority of the pixels without requiring any other ancillary information. A more sophisticated labeling scheme could not be reasonably considered given the processing constraints imposed by the computing resources.

4.1.2. *Output.* The output generated by this algorithm consists in one FAPAR value, one value for the rectified red and near-infrared, respectively. The output field also contains the description of the geometry of illumination and observation, and one flag value for each pixel in the data input stream.

The flag value corresponds to the identification (ID) numbers described in section 4.1.1.

If the ID value is equal to 0, the value of FAPAR is considered valid and the physical range of values lies in between 0 and 1.0.

If the ID number is equal either to 1 ("bad data"), 2 ("cloud, snow and ice") or 3 ("water body and deep shadow"), the value of FAPAR has not been computed and the reported value is equal to its error value.

If the ID number is equal to 4 ("bright surface"), the value has been set at 0.

If ID number is equal to 5 ("undefined"), the value has not been computed and the reported value is set to its error value.

If the ID number is equal to 6, the value was less than 0 and the reported value is equal to 0.

If the ID number is equal to 7, the value was larger than 1 and the reported value is reset to 1.

5. Assumptions and limitations

5.1. **Assumptions.** The following assumptions have been made in the design of the JRC-L7OF:

(1) The spectral reflectances used as input to this algorithm have to be corrected for the seasonally variable distance between the Earth and the Sun.

(2) The plane-parallel approximation for radiation transfer has been assumed to be valid in the atmosphere.

(3) Plant canopies are assumed to be horizontally homogeneous within the Landsat 7 ETM+ pixel.

(4) All orographic effects have been ignored.

(5) Adjacency effects have been ignored.

TABLE 8. Pixel labeling criteria

Identification number (ID)	Spectral tests	Associated categories
0	$0 < \rho_{BLUE} < 0.257752$ and $0 < \rho_{RED} < 0.48407$ and $0 < \rho_{NIR} < 0.683928$ and $0 < \rho_{BLUE} \leq \rho_{NIR}$ and $\rho_{NIR} \geq 1.26826\,\rho_{RED}$	vegetated surface
1	$\rho_{BLUE} \leq 0$ or $\rho_{RED} \leq 0$ or $\rho_{NIR} \leq 0$	bad data
2	$\rho_{BLUE} \geq 0.257752$ or $\rho_{RED} \geq 0.48407$ or $\rho_{NIR} \geq 0.683928$	cloud, snow and ice
3	$0 < \rho_{BLUE} < 0.257752$ and $0 < \rho_{RED} < 0.48407$ and $0 < \rho_{NIR} < 0.683928$ and $\rho_{BLUE} > \rho_{NIR}$	water body and deep shadow
4	$0 < \rho_{BLUE} < 0.257752$ and $0 < \rho_{RED} < 0.48407$ and $0 < \rho_{NIR} < 0.683928$ and $0 < \rho_{BLUE} \leq \rho_{NIR}$ and $1.25\,\rho_{RED} > \rho_{NIR}$	bright surface
5	$\rho_{R_{RED}} < 0$ or $\rho_{R_{NIR}} < 0$	undefined
6	$FAPAR < 0$	no vegetation
7	$FAPAR > 1$	vegetation (out of bounds)

5.2. **Limitations.** The following limitations apply to the algorithm described in this version of the document:

(1) The retrieval of vegetation characteristics in hilly or mountainous regions may or may not be reliable. If the approach turns out to be unreliable in the presence of significant topographical features, additional tests may have to be implemented to screen out these regions on the basis of appropriate Digital Elevation Model (DEM) data. This would imply access to the corresponding elevation data sets, to

reliably navigated LANDSAT data, and the presence of an additional orographic flag.

(2) The optimization of the algorithm was performed using a set of simulated TOA reflectance values which are expected to represent the most commonly encountered geophysical conditions. Although a wide range of possibilities were investigated, there is no guarantee that the most common geophysical scenarios have been implemented.

(3) The sun zenith angle should be lower than 60° (due to the limitation of the radiative transfer models.)

(4) The viewing zenith angle should be smaller than 4°

6. Algorithm requirements

The implementation of the proposed algorithm to estimate FAPAR requires three different types of information, namely, the input data from the Landsat 7 ETM+ sensor, a set of ancillary data and a set of mathematical functions. The ancillary data are the set of coefficients given in Tables 3 to 6. The mathematical functions are given by equations (2), (8), (9) and (13).

The input data are the BRFs measured by the instrument at blue, red and near-infrared bands, together with the geometrical conditions of illumination and observation, namely θ_0, θ_v, ϕ. The sun-sensor relative azimuth, ϕ, is limited to the range [0°, 180°] and the backscatter/hot spot (forwardscatter/specular) direction is defined at 0° (180°).

7. Example of application

The following example shows how the Landsat ETM+ data are processed to compute the FAPAR values. The three bands are found in the following files:

- `p022r032_7t20000917_z16_n10`
- `p022r032_7t20000917_z16_n30`
- `p022r032_7t20000917_z16_n40`

whereas calibration and angles information are stored in the metadata file `p022r032_7t20000917.met`.

Since the data correspond to the digital counts, they are first converted to radiances (following Eq. 23) and used for computing the reflectance factors (BRFs) values using Eq. 24
(see `http://landsathandbook.gsfc.nasa.gov/handbook/handbook_htmls/chapter11/chapter11.html`:

$$R(\lambda) = gain(\lambda) * DN + offset(\lambda) \tag{23}$$

where "gain" and "offset" are given in the associated metadata file.

$$\rho(\lambda) = \frac{\pi * R(\lambda) * dsol^2}{E_0(\lambda) * \cos(\theta_0)} \tag{24}$$

where
θ_0 is the sun zenith angle and $E_0(\lambda)$ is the mean solar exoatmospheric irradiance (in $W/(m^2\,\mu m)$:

$$E_0 = [1969.000, 1840.000, 1551.000, 1044.000] \tag{25}$$

and
dsol the Earth-Sun distance in astronomical units computed with the following equation Eq.26:

$$\begin{aligned} dsol \;=\; & 1.0/((1.00014 - 0.01671\cos(2.0\pi(0.9856002831j - 3.4532868)/360.0) \\ & -0.00014\cos(4.0\pi(0.9856002831j - 3.4532868)/360.0)) \\ & \times(1.00014 - 0.01671\cos(2.0\pi(0.9856002831j - 3.4532868)/360.0) \\ & -0.00014\cos(4.0\pi(0.9856002831j - 3.4532868)/360.0))) \end{aligned}$$

where j is the day of year.

The left image in Figure 7 corresponds to a RGB color image of the Landsat ETM+ data acquired on 17 September 2000. This image surrounds Bondville site (EOS validation site) and shows various land cover type including a large sample of crops. The corresponding rectified channels in red and near-infrared domains are illustrated in the two bottom panels in figure 8 whereas the fapar map is shown in figure 7 (right panel).

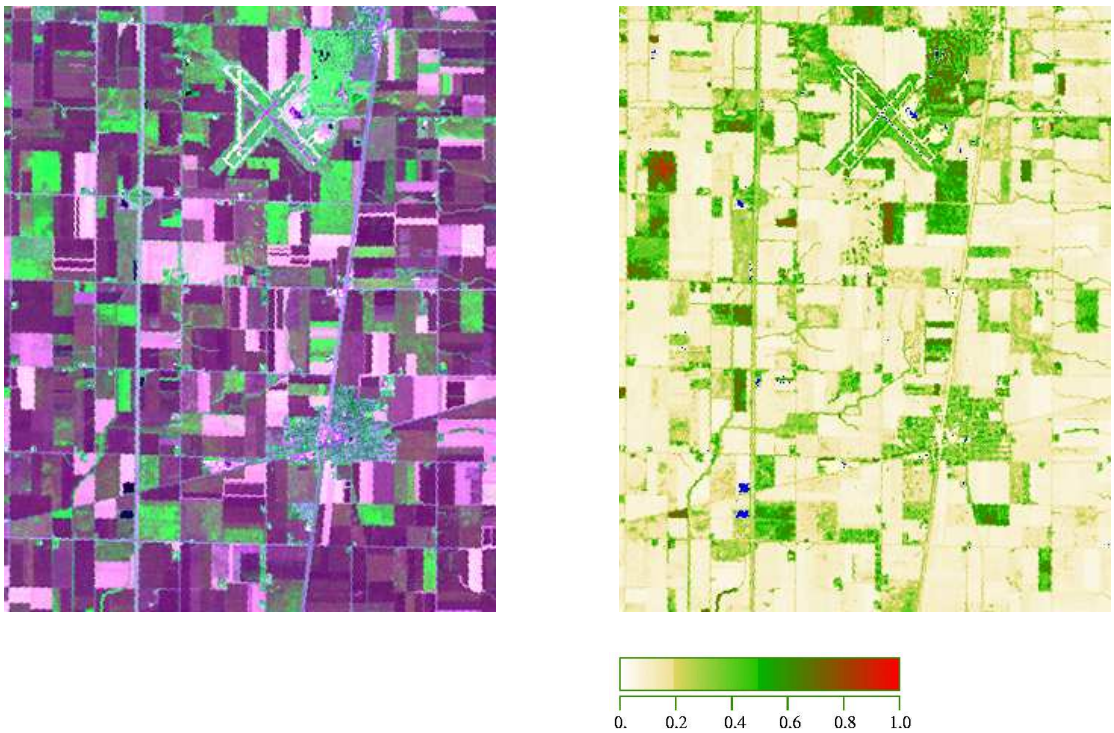

FIGURE 7. Color image (left) and FAPAR map (right) over Bondville - Path 22 - Row 32 taken the 17 Sept. 2000

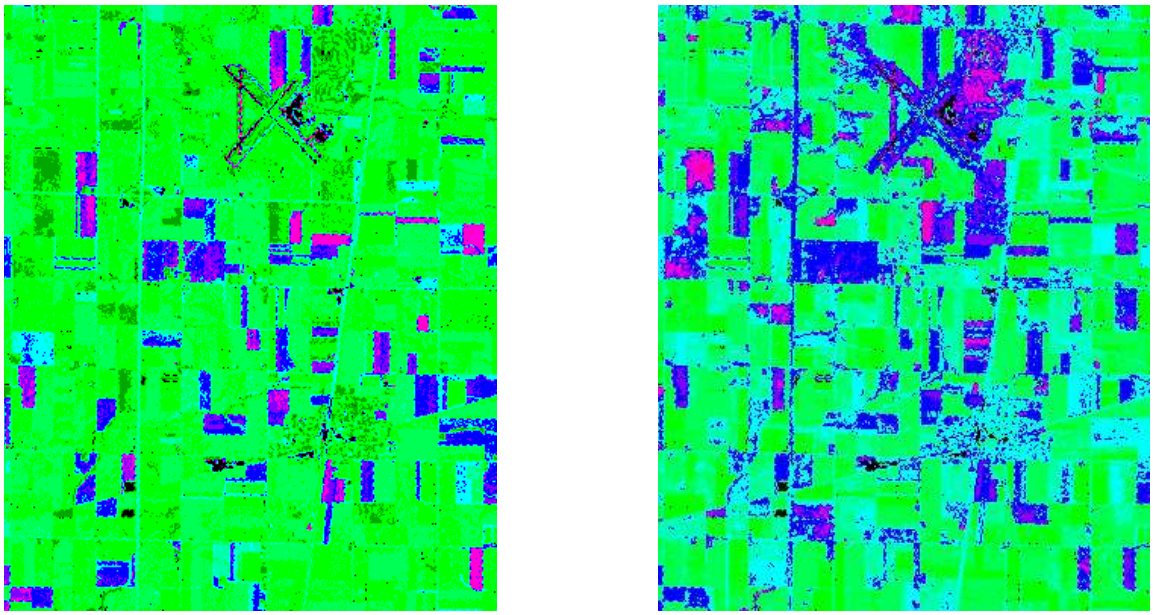

FIGURE 8. Rectified Values in Red and Near-Infrared Channels

References

Gobron, N., O. Aussedat, and P. Bernard (2006a). Moderate Resolution Imaging Spectroradiometer, JRC-FAPAR Algorithm Theoretical Basis Document. EUR Report No. 22164 EN, Institute for Environment and Sustainability.

Gobron, N., O. Aussedat, and P. Bernard (2006b). Moderate Resolution Imaging Spectroradiometer, JRC-FAPAR Algorithm Theoretical Basis Document. EUR Report No. 22164 EN, Institute for Environment and Sustainability.

Gobron, N., O. Aussedat, B. Pinty, M. Taberner, and M. M. Verstraete (2004). Medium Resolution Imaging Spectrometer (MERIS) - Level 2 Land Surface Products - Algorithm Theoretical Basis Document-Revision 3.0. EUR Report No. 21387 EN, Institute for Environment and Sustainability.

Gobron, N., B. Pinty, O. Aussedat, J. M. Chen, W. B. Cohen, R. Fensholt, V. Gond, K. F. Huemmrich, T. Lavergne, F. Mlin, J. L. Privette, I. Sandholt, M. Taberner, D. P. Turner, M. Verstraete, and J.-l. Widlowski (2006). Evaluation of FAPAR Products for Different Canopy Radiation Transfer Regimes: Methodology and Results using JRC Products Derived from SeaWiFS against ground-based estimations. *Journal of Geophysical Research 111*.

Gobron, N., B. Pinty, O. Aussedat, M. Taberner, O. Faber, F. Mélin, T. Lavergne, M. Robustelli, and P. Snoeij (2008). Uncertainty estimates for the FAPAR operational products derived from MERIS - Impact of top-of-atmosphere radiance uncertainties and validation with field data. *Remote Sensing of Environment 112*, 18711883.

Gobron, N., B. Pinty, F. Mélin, M. Taberner, and M. M. Verstraete (2002). Sea Wide Field-of-View Sensor (SeaWiFS) - An optimized FAPAR algorithm - Theoretical Basis Document. EUR Report No. 20148 EN, Institute for Environment and Sustainability.

Gobron, N., B. Pinty, M. M. Verstraete, and Y. Govaerts (1997). A semi-discrete model for the scattering of light by vegetation. *Journal of Geophysical Research 102*, 9431–9446.

Gobron, N., B. Pinty, M. M. Verstraete, and Y. Govaerts (1999). The MERIS Global Vegetation Index (MGVI): description and preliminary application. *International Journal of Remote Sensing 20*, 1917–1927.

Gobron, N., B. Pinty, M. M. Verstraete, and M. Taberner (2002a). Global Land Imager (GLI) - An optimized FAPAR algorithm - Theoretical Basis Document. EUR Report No. 20147 EN, Institute for Environment and Sustainability.

Gobron, N., B. Pinty, M. M. Verstraete, and M. Taberner (2002b). VEGETATION - An optimized FAPAR algorithm - Theoretical Basis Document. EUR Report No. 20146 EN, Institute for Environment and Sustainability.

Gobron, N., B. Pinty, M. M. Verstraete, and J.-L. Widlowski (2000). Advanced spectral algorithm and new vegetation indices optimized for up coming sensors: Development, accuracy and applications. *IEEE Transactions on Geoscience and Remote Sensing 38*, 2489–2505.

Govaerts, Y., M. M. Verstraete, B. Pinty, and N. Gobron (1999). Designing optimal spectral indices: a feasibility and proof of concept study. *International Journal of Remote Sensing 20*, 1853–1873.

Jacquemoud, S. and F. Baret (1990). PROSPECT: A model of leaf optical properties spectra. *Remote Sensing of Environment 34*, 75–91.

Leprieur, C., M. M. Verstraete, and B. Pinty (1994). Evaluation of the performance of various vegetation indices to retrieve vegetation cover from AVHRR data. *Remote Sensing Reviews 10*, 265–284.

Price, J. C. (1995). Examples of high resolution visible to near-infrared reflectance spectra and a standardized collection for remote sensing studies. *International Journal of Remote Sensing 16*, 993–1000.

Rahman, H., B. Pinty, and M. M. Verstraete (1993). Coupled surface-atmosphere reflectance (CSAR) model. 2. Semiempirical surface model usable with NOAA Advanced Very High Resolution Radiometer data. *Journal of Geophysical Research 98*, 20,791–20,801.

Vermote, E., D. Tanré, J. L. Deuzé, M. Herman, and J. J. Morcrette (1997). Second simulation of the satellite signal in the solar spectrum: An overview. *IEEE Trans. Geoscience Remote Sensing 35-3*, 675–686.

Verstraete, M. M. and B. Pinty (1996). Designing optimal spectral indices for remote sensing applications. *IEEE Transactions on Geoscience and Remote Sensing 34*, 1254–1265.

European Commission

EUR 23554 - Joint Research Centre - Institute for Environment and Sustainability
Title: Landsat 7 Enhanced Thematic Mapper JRC-FAPAR - Algorithm Theoretical Basis Document.
Author(s): Nadine Gobron and Malcolm Taberner
Luxembourg: Office for Official Publications of the European Communities
2008 - 27 pp.
EUR - Scientific and Technical Research series - ISSN 1018-5593

Abstract

This Algorithm Theoretical Basis document (ATBd) describes the Joint Research Center (JRC)- procedure used to retrieve information of absorbed photosynthetical radiation by the vegetated terrestrial surfaces from an analysis of the Top Of Atmosphere (TOA) data acquired by the Landsat 7 Enhanced Thematic Mapper (ETM+) instrument. The corresponding data consist of eight spectral bands, with a spatial resolution of 30 meters for bands 1 to 5 and band 7 whereas the resolution for band 6 (thermal infrared) is 60 meters and resolution for band 8 (panchromatic) is 15 meters. Approximate scene size is 170 km north-south by 183 km east-west.

The code of the proposed algorithm takes the form of a set of several formulae which transform calibrated spectral directional reflectances into a single numerical value. These formulae are designed to extract the Fraction of Absorbed Photosynthetically Active Radiation (FAPAR) in the plant canopy from the measurements. The methodology described in this document has been optimized to assess the presence on the ground of healthy live green vegetation. The optimization procedure has been constrained to provide an estimate of FAPAR in the plant canopy, although the outputs are expected to be used in a wide range of applications. This algorithm delivers, in addition to the FAPAR product, the so-called rectified reflectance values in the red and near-infrared spectral bands (Landsat 7 ETM+ Band 3 and Band 4). These are virtual reflectances largely decontaminated from atmospheric and angular effects. It also provides a categorization of pixel types thanks to a pre-processing identification based on multi-spectral properties.

The mission of the JRC is to provide customer-driven scientific and technical support for the conception, development, implementation and monitoring of EU policies. As a service of the European Commission, the JRC functions as a reference centre of science and technology for the Union. Close to the policy-making process, it serves the common interest of the Member States, while being independent of special interests, whether private or national.